8

Flux Vector Splitting Methods

8.1 Introduction

A distinguishing feature of upwind numerical methods is this: *the discretisation of the equations on a mesh is performed according to the direction of propagation of information on that mesh.* In this way, salient features of the physical phenomena modelled by the equations are incorporated into the discretisation schemes. There are essentially two approaches for identifying upwind directions, namely the *Godunov approach* [216] studied in Chap. 6, and the *Flux Vector Splitting* (FVS) approach [424], [463], [560], [561] to be studied in this chapter. These two approaches are often referred to as the *Riemann approach* and the *Boltzmann approach* [244]. The respective numerical methods derived from these two approaches are often referred to as *Flux Difference Splitting Methods* and *Flux Vector Splitting Methods* . For a review on both of these approaches the paper by Harten, Lax and van Leer [244] is highly recommended. Closely related schemes to FVS, not studied here, are the KFVS or kinetic schemes, see for example Pullin [389], Perthame [380], [381], Mandal and Desphande [336], Xu and Prendergast [587], Xu et. al. [586], Xu [585] and Yang *et. al* [591].

The identification of upwind directions in Flux Vector Splitting Methods is achieved with less effort than in Godunov–type methods, leading to simpler and somewhat more efficient schemes. These two features are very attractive and have made FVS schemes very popular within a large community of practitioners. The Flux Vector Splitting approach is particularly well suited for *implicit methods*; these are popular in Aerodynamics, where the computation of steady solutions is of great practical value. The reduced sophistication of FVS schemes however, as compared with Godunov–type schemes, results in poorer resolution of discontinuities, particularly stationary contact and shear waves. In applications to the Navier–Stokes equations, it is reported by van Leer, Thomas and Roe [565] that their FVS scheme is considerably less accurate than Godunov's method with Roe's approximate Riemann solver [407]. A key feature of the FVS approach is its reliance on a special property of the

E.F. Toro, *Riemann Solvers and Numerical Methods for Fluid Dynamics*,
DOI 10.1007/b7976-1_8,

equations, namely the *homogeneity property*. As seen in Sect. 3.1.1 of Chap. 3, the Euler equations satisfy this property but there are important examples, such as the shallow water equations, that do not. The homogeneity property may however be circumvented so as to be able to apply the FVS approach, see Vázquez–Cendón [568].

The pioneering works of Sanders and Prendergast [424], Steger and Warming [463] and van Leer [560], [561] has been followed by numerous applications as well as by increased research efforts to improve further the technique. See for example the papers [12], [13], [166], [328], [578] and [387], amongst many others.

The purpose of this chapter is to give an elementary introduction to Flux Vector Splitting methods. Sects. 8.2 and 8.3 are devoted to a simple introduction to the FVS approach. In Sect. 8.4 we derive FVS methods for the time–dependent Euler equations following the methodologies of Steger and Warming [463], that of van Leer [560], [561] and the recently proposed approach of Liou and Steffen [328]. Numerical results are presented in Sect. 8.5. Techniques to construct high–order schemes based on FVS are found in Chaps. 13 and 14. In Chap. 15 we show how to solve systems with source terms and in Chap. 16 we deal with approaches to construct multidimensional schemes. Essential background material for reading this chapter is found in Chaps. 2, 3 and 5.

8.2 The Flux Vector Splitting Approach

In this section we introduce the flux vector splitting approach in the simple setting of model hyperbolic systems, namely the small perturbation steady supersonic equations and the isothermal equations of Gas Dynamics; see Sect. 1.6.2 of Chap. 1 and Sects. 2.1 and 2.4.1 of Chap. 2 for details on these systems.

8.2.1 Upwind Differencing

Consider the small perturbation steady supersonic equations

$$u_x - a^2 v_y = 0 \ , \ v_x - u_y = 0 \ , \tag{8.1}$$

where $u = u(x, y)$, $v = v(x, y)$,

$$a = \sqrt{\frac{1}{M_\infty^2 - 1}} \tag{8.2}$$

is the sound speed and M_∞ is the free–stream Mach number, assumed to be greater than unity. Equations (8.1) may be rewritten as

$$\mathbf{U}_x + \mathbf{A}\mathbf{U}_y = \mathbf{0} \ , \tag{8.3}$$

with

$$\mathbf{U} = \begin{bmatrix} u \\ v \end{bmatrix} \ , \ \mathbf{A} = \begin{bmatrix} 0 & -a^2 \\ -1 & 0 \end{bmatrix} \ . \tag{8.4}$$

The eigenvalues of the coefficient matrix $\mathbf{A}$ are

$$\lambda_1 = -a \ , \ \lambda_2 = +a \ , \tag{8.5}$$

with corresponding right eigenvectors

$$\mathbf{K}^{(1)} = \begin{bmatrix} a \\ 1 \end{bmatrix} \ , \quad \mathbf{K}^{(2)} = \begin{bmatrix} a \\ -1 \end{bmatrix} \ . \tag{8.6}$$

Given the mixed character of the eigenvalues ($\lambda_1 = -a$ is negative and $\lambda_2 = +a$ is positive), a finite difference discretisation of (8.3) has limited choices for the spatial derivative, if upwind bias is to be applied. Consider, for instance, the *one–sided difference schemes*

$$\mathbf{U}_i^{n+1} = \mathbf{U}_i^n - \frac{\Delta x}{\Delta y}\mathbf{A}[\mathbf{U}_i^n - \mathbf{U}_{i-1}^n] \ , \tag{8.7}$$

$$\mathbf{U}_i^{n+1} = \mathbf{U}_i^n - \frac{\Delta x}{\Delta y}\mathbf{A}[\mathbf{U}_{i+1}^n - \mathbf{U}_i^n] \ . \tag{8.8}$$

Clearly scheme (8.7) is upwind relative to the eigenvalue $\lambda_2 = a > 0$ but is downwind, and thus unstable, relative to the eigenvalue $\lambda_1 = -a < 0$. A similar observation applies to scheme (8.8). For the case in which all eigenvalues have the same sign the difficulty of choosing the upwind direction does not arise.

As seen in Sect. 5.4 of Chap. 5, general linear hyperbolic systems with constant coefficients may be solved by the CIR first–order upwind method by decomposing the coefficient matrix $\mathbf{A}$ into a positive component $\mathbf{A}^+$ and a negative component $\mathbf{A}^-$, such that

$$\mathbf{A} = \mathbf{A}^+ + \mathbf{A}^- \ , \tag{8.9}$$

where $\mathbf{A}^+$ has positive or zero eigenvalues and $\mathbf{A}^-$ has negative or zero eigenvalues. One then has the upwind scheme

$$\mathbf{U}_i^{n+1} = \mathbf{U}_i^n - \frac{\Delta x}{\Delta y}\mathbf{A}^+[\mathbf{U}_i^n - \mathbf{U}_{i-1}^n] - \frac{\Delta x}{\Delta y}\mathbf{A}^-[\mathbf{U}_{i+1}^n - \mathbf{U}_i^n] \ . \tag{8.10}$$

The *Split–Coefficient Matrix Scheme* of Chakravarthy et. al. [97], [251] is an extension of this procedure to non–linear systems, in non–conservative form.

The CIR upwind scheme, when applied to general linear hyperbolic systems with constant coefficients, may be written in conservative form by defining the flux vector

$$\mathbf{F} = \mathbf{A}\mathbf{U} \ . \tag{8.11}$$

Then the splitting (8.9) of the coefficient matrix $\mathbf{A}$ results in a natural splitting of the flux vector $\mathbf{F}$, namely

$$\mathbf{F} = \mathbf{F}^+ + \mathbf{F}^- \,. \tag{8.12}$$

In this way the CIR upwind scheme can be written in conservative form

$$\mathbf{U}_i^{n+1} = \mathbf{U}_i^n - \frac{\Delta t}{\Delta x}[\mathbf{F}_{i+\frac{1}{2}} - \mathbf{F}_{i-\frac{1}{2}}] \,, \tag{8.13}$$

where the intercell numerical flux

$$\mathbf{F}_{i+\frac{1}{2}} = \mathbf{F}_i^+(\mathbf{U}_i^n) + \mathbf{F}_i^-(\mathbf{U}_{i+1}^n) \tag{8.14}$$

is identical to the Godunov intercell flux. See Sect. 5.4 of Chap. 5 for details. The Flux Vector Splitting Method is a generalisation of this to non–linear systems in conservation form.

8.2.2 The FVS Approach

Here we consider a general system of m non–linear hyperbolic conservation laws

$$\mathbf{U}_t + \mathbf{F}(\mathbf{U})_x = \mathbf{0} \,. \tag{8.15}$$

From the assumption of hyperbolicity the Jacobian matrix

$$\mathbf{A}(\mathbf{U}) = \frac{\partial \mathbf{F}}{\partial \mathbf{U}} \tag{8.16}$$

may be expressed as

$$\mathbf{A} = \mathbf{K}\mathbf{\Lambda}\mathbf{K}^{-1} \,, \tag{8.17}$$

where $\mathbf{\Lambda}$ is the diagonal matrix formed by the eigenvalues of $\mathbf{A}$, namely

$$\mathbf{\Lambda} = \begin{bmatrix} \lambda_1 & & 0 \\ & \ddots & \\ 0 & & \lambda_m \end{bmatrix} \,. \tag{8.18}$$

The matrix $\mathbf{K}$ is

$$\mathbf{K} = [\mathbf{K}^{(1)}, \mathbf{K}^{(2)}, \ldots, \mathbf{K}^{(m)}] \,, \tag{8.19}$$

where the column $\mathbf{K}^{(i)}$ is the right eigenvector of $\mathbf{A}$ corresponding to λ_i and $\mathbf{K}^{-1}$ is the inverse of $\mathbf{K}$. Recall our usual convention of ordering the eigenvalues in *increasing* order.

As anticipated in the previous section, the Flux Vector Splitting method aims at generalising (8.14) to non–linear systems (8.15). That is, FVS requires a splitting of the flux vector $\mathbf{F}$ into two component $\mathbf{F}^+$ and $\mathbf{F}^-$ such that

$$\mathbf{F}(\mathbf{U}) = \mathbf{F}^+(\mathbf{U}) + \mathbf{F}^-(\mathbf{U}) \,, \tag{8.20}$$

under the restriction that the eigenvalues $\hat{\lambda}_i^+$ and $\hat{\lambda}_i^-$ of the Jacobian matrices

$$\hat{\mathbf{A}}^+ = \frac{\partial \mathbf{F}^+}{\partial \mathbf{U}} \,, \quad \hat{\mathbf{A}}^- = \frac{\partial \mathbf{F}^-}{\partial \mathbf{U}} \tag{8.21}$$

satisfy the condition

$$\hat{\lambda}_i^+ \geq 0 \,, \quad \hat{\lambda}_i^- \leq 0 \,. \tag{8.22}$$

The splitting is also required to reproduce *regular upwinding* when all eigenvalues λ_i of the coefficient matrix $\mathbf{A}$ are one–sided, that is, all positive or zero, or all negative or zero. That is to say

$$\left.\begin{aligned} &\mathbf{F}^+ = \mathbf{F} \,, \quad \mathbf{F}^- = \mathbf{0} \quad \text{if } \lambda_i \geq 0 \quad \text{for } i = 1, \ldots, m \,, \\ &\mathbf{F}^+ = \mathbf{0} \,, \quad \mathbf{F}^- = \mathbf{F} \quad \text{if } \lambda_i \leq 0 \quad \text{for } i = 1, \ldots, m \,. \end{aligned}\right\} \tag{8.23}$$

If in addition to hyperbolicity, the system (8.15) satisfies the *homogeneity property*

$$\mathbf{F}(\mathbf{U}) = \mathbf{A}(\mathbf{U})\mathbf{U} \,, \tag{8.24}$$

just as in the linear constant coefficient case, then the sought splitting is easily accomplished by identifying a suitable splitting of the Jacobian matrix $\mathbf{A}$. As seen in Sect. 3.1.1 of Chap. 3, the time–dependent Euler equations satisfy the *homogeneity property*.

From the diagonalisation of $\mathbf{A}$ given by (8.17), a splitting of $\mathbf{A}$ may be accomplished by an appropriate splitting of the diagonal matrix $\mathbf{\Lambda}$. This in turn, may be split by identifying a splitting of the eigenvalues λ_i, $i = 1, \ldots, m$ of $\mathbf{A}$. Suppose we may split the eigenvalues λ_i as

$$\lambda_i = \lambda_i^+ + \lambda_i^- \,, \tag{8.25}$$

such that $\lambda_i^+ \geq 0$ and $\lambda_i^- \leq 0$. Then $\mathbf{\Lambda}$ may be split as

$$\mathbf{\Lambda} = \mathbf{\Lambda}^+ + \mathbf{\Lambda}^- \,, \tag{8.26}$$

where

$$\mathbf{\Lambda}^+ = \begin{bmatrix} \lambda_1^+ & & 0 \\ & \ddots & \\ 0 & & \lambda_m^+ \end{bmatrix} \,, \quad \mathbf{\Lambda}^- = \begin{bmatrix} \lambda_1^- & & 0 \\ & \ddots & \\ 0 & & \lambda_m^- \end{bmatrix} \,. \tag{8.27}$$

A natural splitting of $\mathbf{A}$ results, namely

$$\mathbf{A} = \mathbf{A}^+ + \mathbf{A}^- \,, \tag{8.28}$$

with

$$\mathbf{A}^+ = \mathbf{K}\mathbf{\Lambda}^+\mathbf{K}^{-1} \,, \quad \mathbf{A}^- = \mathbf{K}\mathbf{\Lambda}^-\mathbf{K}^{-1} \,. \tag{8.29}$$

Then, if (8.24) is satisfied, we can split $\mathbf{F}(\mathbf{U})$ as

$$\mathbf{F} = \mathbf{F}^+ + \mathbf{F}^- \,, \tag{8.30}$$

where

$$\mathbf{F}^+ = \mathbf{A}^+\mathbf{U}\,, \quad \mathbf{F}^- = \mathbf{A}^-\mathbf{U}\,. \tag{8.31}$$

Steger and Warming [463] proposed a splitting of the eigenvalues λ_i as in (8.25) with definitions

$$\lambda_i^+ = \frac{1}{2}(\lambda_i + \mid \lambda_i \mid)\,, \quad \lambda_i^- = \frac{1}{2}(\lambda_i - \mid \lambda_i \mid)\,, \tag{8.32}$$

where $\mid \lambda_i \mid$ is the absolute value of λ_i namely,

$$\mid \lambda_i \mid = \begin{cases} \lambda_i \;\; if\ \lambda_i \geq 0\,, \\ -\lambda_i \; if\ \lambda_i \leq 0\,. \end{cases} \tag{8.33}$$

Clearly

$$\lambda_i^+ \geq 0\,, \quad \lambda_i^- \leq 0\,, \quad for\ i = 1, \ldots, m. \tag{8.34}$$

Exercise 8.1. Verify that the following properties are satisfied

$$\left.\begin{array}{l} \lambda_i = \lambda_i^+ + \lambda_i^- \;\; ; \;\; \mid \lambda_i \mid = \lambda_i^+ - \lambda_i^-\,, \\ \mathbf{\Lambda} = \mathbf{\Lambda}^+ + \mathbf{\Lambda}^- \;\; ; \;\; \mid \mathbf{\Lambda} \mid = \mathbf{\Lambda}^+ - \mathbf{\Lambda}^-\,, \\ \mathbf{A} = \mathbf{A}^+ + \mathbf{A}^- \;\; ; \;\; \mid \mathbf{A} \mid = \mathbf{A}^+ - \mathbf{A}^-\,. \end{array}\right\} \tag{8.35}$$

Solution 8.2. (Left to the reader).

8.3 FVS for the Isothermal Equations

In order to illustrate the FVS approach we consider the isothermal equations of Gas Dynamics

$$\mathbf{U}_t + \mathbf{F}(\mathbf{U})_x = \mathbf{0}\,, \tag{8.36}$$

$$\mathbf{U} = \begin{bmatrix} \rho \\ \rho u \end{bmatrix}\,, \quad \mathbf{F}(\mathbf{U}) = \begin{bmatrix} \rho u \\ \rho u^2 + \rho a^2 \end{bmatrix}\,, \tag{8.37}$$

where the sound speed a is a positive constant. For details on the eigenstructure of this system see Sect. 2.4 of Chap. 2. The Jacobian matrix is

$$\mathbf{A} = \frac{\partial \mathbf{F}}{\partial \mathbf{U}} = \begin{bmatrix} 0 & 1 \\ a^2 - u^2 & 2u \end{bmatrix}\,. \tag{8.38}$$

The eigenvalues of $\mathbf{A}$ are

$$\lambda_1 = u - a\,, \quad \lambda_2 = u + a \tag{8.39}$$

and the matrix $\mathbf{K}$ of corresponding right eigenvectors is

$$\mathbf{K} = \begin{bmatrix} 1 & 1 \\ u - a & u + a \end{bmatrix}\,. \tag{8.40}$$

Exercise 8.3. Verify that system (8.36)–(8.37) satisfy the *homogeneity property* (8.24).

Solution 8.4. (Left to the reader).

8.3.1 Split Fluxes

Given any splitting (8.25) with

$$\mathbf{\Lambda}^+ = \begin{bmatrix} \lambda_1^+ & 0 \\ 0 & \lambda_2^+ \end{bmatrix} , \quad \mathbf{\Lambda}^- = \begin{bmatrix} \lambda_1^- & 0 \\ 0 & \lambda_2^- \end{bmatrix} , \tag{8.41}$$

we require the computation of the matrices $\mathbf{A}^+$ and $\mathbf{A}^-$ as given by (8.29). One then requires the determination of the inverse $\mathbf{K}^{-1}$ of the matrix $\mathbf{K}$, the products of three matrices as in (8.29) and finally the products (8.31) to find the flux components. For large systems this may be a rather tedious algebraic task. For the isothermal equations we have

$$\mathbf{K}^{-1} = \frac{1}{2a} \begin{bmatrix} u+a & -1 \\ a-u & 1 \end{bmatrix} . \tag{8.42}$$

Now, given any of the two components (8.27) of $\mathbf{\Lambda}$, $\mathbf{A}^\alpha$, say, we compute

$$\mathbf{A}^\alpha = \mathbf{K}\mathbf{\Lambda}^\alpha\mathbf{K}^{-1} .$$

The result is

$$\mathbf{A}^\alpha = \frac{1}{2a} \begin{bmatrix} \lambda_1^\alpha(u+a) - \lambda_2^\alpha(u-a) & \lambda_2^\alpha - \lambda_1^\alpha \\ (u^2-a^2)(\lambda_1^\alpha - \lambda_2^\alpha) & \lambda_2^\alpha(u+a) - \lambda_1^\alpha(u-a) \end{bmatrix} . \tag{8.43}$$

Application of (8.31) gives the flux vector component

$$\mathbf{F}^\alpha = \mathbf{A}^\alpha\mathbf{U} ,$$

that is

$$\mathbf{F}^\alpha = \frac{\rho}{2} \begin{bmatrix} \lambda_1^\alpha + \lambda_2^\alpha \\ \lambda_1^\alpha(u-a) + \lambda_2^\alpha(u+a) \end{bmatrix} . \tag{8.44}$$

Note that the expression for the component $\mathbf{F}^\alpha$ given by (8.44) is general. For $\alpha = +$ and $\alpha = -$ the flux components $\mathbf{F}^+$ and $\mathbf{F}^-$ are

$$\mathbf{F}^+ = \frac{\rho}{2} \begin{bmatrix} \lambda_1^+ + \lambda_2^+ \\ \lambda_1^+(u-a) + \lambda_2^+(u+a) \end{bmatrix} , \tag{8.45}$$

and

$$\mathbf{F}^- = \frac{\rho}{2} \begin{bmatrix} \lambda_1^- + \lambda_2^- \\ \lambda_1^-(u-a) + \lambda_2^-(u+a) \end{bmatrix} . \tag{8.46}$$

Exercise 8.5. For the split fluxes (8.45)–(8.46), for the case of subsonic flow,

– (i) Find the Jacobian matrices

$$\hat{\mathbf{A}}^+ = \frac{\partial \mathbf{F}^+}{\partial \mathbf{U}} , \quad \hat{\mathbf{A}}^- = \frac{\partial \mathbf{F}^-}{\partial \mathbf{U}} .$$

– (ii) Find the eigenvalues $\hat{\lambda}_i^+$ and $\hat{\lambda}_i^-$.

Solution 8.6. For the positive flux component $\mathbf{F}^+$ the Jacobian matrix is

$$\hat{\mathbf{A}}^+ = \frac{\partial \mathbf{F}^+}{\partial \mathbf{U}} = \begin{bmatrix} \frac{1}{2}a & \frac{1}{2} \\ \frac{1}{2}(a^2 - u^2) & u + a \end{bmatrix} .$$

The eigenvalues are the roots of the characteristic polynomial

$$\lambda^2 - (\frac{3}{2}a + u)\lambda + \frac{1}{4}(u + a)^2 = 0 ,$$

namely,

$$\hat{\lambda}_1^+ = \frac{1}{4}a\left[2M + 3 - \sqrt{4M + 5}\right] , \quad \hat{\lambda}_2^+ = \frac{1}{4}a\left[2M + 3 + \sqrt{4M + 5}\right] .$$

Remark 8.7. Note that

$$\hat{\mathbf{A}}^+ \neq \mathbf{A}^+$$

and that

$$\hat{\lambda}_i^+ \neq \lambda_i^+ .$$

Note also that $\hat{\lambda}_i^+ > 0$, that is, none of the eigenvalues vanish. Numerically, this particular property is not desirable, and which unfortunately also carries over to the Euler equations. As we shall see in the next section, there are other splitting schemes that remove this difficulty.

8.3.2 FVS Numerical Schemes

The FVS approach can be used to solve (8.36) using the *explicit* conservative scheme

$$\mathbf{U}_i^{n+1} = \mathbf{U}_i^n - \frac{\Delta t}{\Delta x}[\mathbf{F}_{i+\frac{1}{2}} - \mathbf{F}_{i-\frac{1}{2}}] , \tag{8.47}$$

where the FVS numerical flux is given by

$$\mathbf{F}_{i+\frac{1}{2}} = \mathbf{F}_i^+(\mathbf{U}_i^n) + \mathbf{F}_{i+1}^-(\mathbf{U}_{i+1}^n) . \tag{8.48}$$

Fig. 8.1 provides a physical interpretation of (8.48). The intercell numerical flux $\mathbf{F}_{i+\frac{1}{2}}$ is made out from two contributions; one comes from the *forward* component $\mathbf{F}_i^+$ in the *left cell* I_i and the other comes from the *backward* component $\mathbf{F}_{i+1}^-$ in the *right cell* I_{i+1}.

The Steger and Warming [463] splitting (8.32) in a computational set up is as follows: we consider a computing cell I_i at time level n, where $\mathbf{U}_i^n$ is the vector of conserved variables and $\mathbf{F}_i^n \equiv \mathbf{F}(\mathbf{U}_i^n)$ is the vector of fluxes. The three cases to consider are illustrated in Fig. 8.2 and are

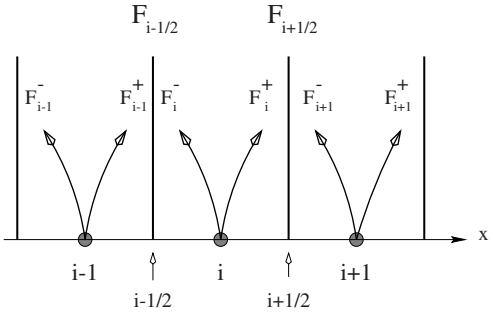

Fig. 8.1. Splitting of the flux function *within* each computing cell I_i at time level n

– Case (a) Left supersonic flow: $\lambda_2 = u_i^n + a_i^n \leq 0$. Fig. 8.2a illustrates the situation in a cell I_i at time level n. Clearly

$$\left.\begin{array}{l} \lambda_1^+ = 0 \ , \lambda_1^- = \lambda_1 = u_i^n - a_i^n \ , \\ \lambda_2^+ = 0 \ , \lambda_2^- = \lambda_2 = u_i^n + a_i^n \ , \\ \mathbf{F}_i^+ = \mathbf{0} \ , \mathbf{F}_i^- = \mathbf{F}_i^n \ . \end{array}\right\} \tag{8.49}$$

– Case (b) Right supersonic flow: $\lambda_1 = u_i^n - a_i^n \geq 0$. See Fig. 8.2b. Obviously

$$\left.\begin{array}{l} \lambda_1^+ = \lambda_1 = u_i^n - a_i^n \ , \lambda_1^- = 0 \ , \\ \lambda_2^+ = \lambda_2 = u_i^n + a_i^n \ , \lambda_2^- = 0 \ , \\ \mathbf{F}_i^+ = \mathbf{F}_i^n \qquad\qquad , \mathbf{F}_i^- = \mathbf{0} \ . \end{array}\right\} \tag{8.50}$$

– Case (c) Subsonic flow: $\lambda_1 = u_i^n - a_i^n \leq 0 \leq \lambda_2 = u_i^n + a_i^n$. See Fig. 8.2c. Evidently

$$\left.\begin{array}{l} \lambda_1^+ = 0 \qquad\qquad , \lambda_1^- = \lambda_1 = u_i^n - a_i^n \ , \\ \lambda_2^+ = \lambda_2 = u_i^n + a_i^n \ , \lambda_2^- = 0 \ . \end{array}\right\} \tag{8.51}$$

According to (8.45)–(8.46) the fluxes $\mathbf{F}_i^+$ and $\mathbf{F}_i^-$ for the subsonic case are given by

$$\mathbf{F}_i^+ = \frac{\rho_i^n}{2} \begin{bmatrix} u_i^n + a_i^n \\ (u_i^n + a_i^n)^2 \end{bmatrix} \ , \quad \mathbf{F}_i^- = \frac{\rho_i^n}{2} \begin{bmatrix} u_i^n - a_i^n \\ (u_i^n - a_i^n)^2 \end{bmatrix} \ . \tag{8.52}$$

8.4 FVS Applied to the Euler Equations

Here we present three Flux Vector Splitting schemes applied to the time dependent Euler equations.

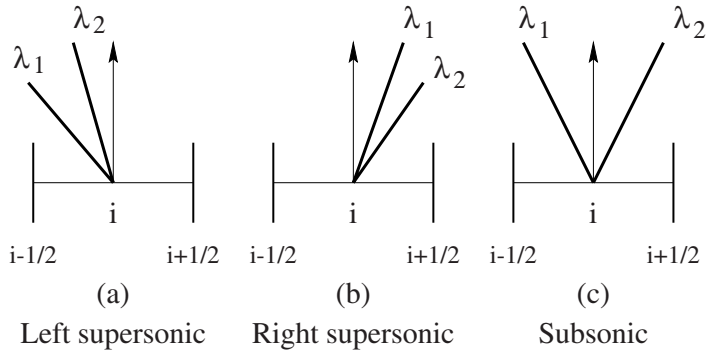

Fig. 8.2. Possible flow patterns in cell I_i at time n: (a) supersonic flow to the left (b) supersonic flow to the right (c) subsonic flow

8.4.1 Recalling the Equations

The one–dimensional Euler Equations in conservation–law form are given by

$$\mathbf{U}_t + \mathbf{F}(\mathbf{U})_x = \mathbf{0}\,, \tag{8.53}$$

$$\mathbf{U} = \begin{bmatrix} \rho \\ \rho u \\ E \end{bmatrix}\,, \quad \mathbf{F}(\mathbf{U}) = \begin{bmatrix} \rho u \\ \rho u^2 + p \\ u(E+p) \end{bmatrix}\,. \tag{8.54}$$

As seen in Sect. 3.1.1 of Chap. 3, the Jacobian matrix $\mathbf{A}$ is given by

$$\mathbf{A} = \begin{bmatrix} 0 & 1 & 0 \\ \frac{1}{2}(\gamma-3)u^2 & (3-\gamma)u & \gamma-1 \\ \frac{1}{2}(\gamma-2)u^3 - \frac{a^2 u}{\gamma-1} & \frac{3-2\gamma}{2}u^2 + \frac{a^2}{\gamma-1} & \gamma u \end{bmatrix} \tag{8.55}$$

and the system is hyperbolic with real eigenvalues

$$\lambda_1 = u - a\,,\ \lambda_2 = u\,,\ \lambda_3 = u + a\,. \tag{8.56}$$

The matrix $\mathbf{K}$ of corresponding right eigenvectors is

$$\mathbf{K} = \begin{bmatrix} 0 & 1 & 0 \\ u-a & u & u+a \\ H - ua & \frac{1}{2}u^2 & H + ua \end{bmatrix}\,. \tag{8.57}$$

Here H is the enthalpy

$$H = (E+p)/\rho = \frac{1}{2}u^2 + \frac{a^2}{(\gamma-1)}\,. \tag{8.58}$$

As explained in Sect. 3.2.4 of Chap. 3, the three–dimensional Euler equations may be dealt with by only considering the flux component *normal* to

the computing cell interface, see also Sect. 16.2 of Chap. 16. In constructing numerical methods for Cartesian geometries it is sufficient to consider the flux in any of the coordinate directions. For general geometries this is modified by use of rotation matrices; see Sect. 3.2 of Chap. 3. We thus state the schemes for the x–split three dimensional Euler equations

$$\mathbf{U}_t + \mathbf{F}(\mathbf{U})_x = \mathbf{0} \,, \tag{8.59}$$

$$\mathbf{U} = \begin{bmatrix} \rho \\ \rho u \\ \rho v \\ \rho w \\ E \end{bmatrix} \,, \quad \mathbf{F}(\mathbf{U}) = \begin{bmatrix} \rho u \\ \rho u^2 + p \\ \rho uv \\ \rho uw \\ u(E+p) \end{bmatrix} \,. \tag{8.60}$$

The Jacobian matrix $\mathbf{A}$, see Sect. 3.2.2 of Chap. 3, is given by

$$\mathbf{A} = \begin{bmatrix} 0 & 1 & 0 & 0 & 0 \\ \hat{\gamma}H - u^2 - a^2 & (3-\gamma)u & -\hat{\gamma}v & -\hat{\gamma}w & \hat{\gamma} \\ -uv & v & u & 0 & 0 \\ -uw & w & 0 & u & 0 \\ \frac{1}{2}u[(\gamma-3)H - a^2] & H - \hat{\gamma}u^2 & -\hat{\gamma}uv & -\hat{\gamma}uw & \gamma u \end{bmatrix} \,, \tag{8.61}$$

where

$$H = (E+p)/\rho = \frac{1}{2}\mathbf{V}^2 + \frac{a^2}{(\gamma-1)} \,, \quad \mathbf{V}^2 = u^2 + v^2 + w^2 \,, \; \hat{\gamma} = \gamma - 1 \,. \tag{8.62}$$

This system is hyperbolic with real eigenvalues

$$\lambda_1 = u - a \,, \; \lambda_2 = \lambda_3 = \lambda_4 = u \,, \; \lambda_5 = u + a \,. \tag{8.63}$$

The matrix of corresponding right eigenvectors is

$$\mathbf{K} = \begin{bmatrix} 1 & 1 & 0 & 0 & 1 \\ u-a & u & 0 & 0 & u+a \\ v & v & 1 & 0 & v \\ w & w & 0 & 1 & w \\ H - ua & \frac{1}{2}\mathbf{V}^2 & v & w & H + ua \end{bmatrix} \tag{8.64}$$

As seen in Chap. 3 the one–dimensional Euler equations satisfy the *homogeneity property*

$$\mathbf{F}(\mathbf{U}) = \mathbf{A}(\mathbf{U})\mathbf{U} \,. \tag{8.65}$$

Exercise 8.8. Verify that the split three–dimensional Euler equations (8.59)–(8.60) also satisfy the homogeneity property (8.65).

Solution 8.9. (Left to the reader).

8.4.2 The Steger–Warming Splitting

For a splitting (8.25)–(8.27) we require an expression for the inverse $\mathbf{K}^{-1}$ of the matrix $\mathbf{K}$, in order to find the split Jacobians (8.29).

The One–Dimensional Case

For the one–dimensional Euler equations we have

$$\mathbf{K}^{-1} = \frac{(\gamma-1)}{2a^2}\begin{bmatrix} \frac{1}{2}u^2 + \frac{ua}{\gamma-1} & -u - \frac{a}{\gamma-1} & 1 \\ \frac{2a^2}{\gamma-1} - u^2 & 2u & -2 \\ \frac{1}{2}u^2 - \frac{ua}{\gamma-1} & \frac{a}{\gamma-1} - u & 1 \end{bmatrix} . \tag{8.66}$$

Then, for any component $\mathbf{\Lambda}^\alpha$ of the two components of $\mathbf{\Lambda}$ in (8.26) the corresponding Jacobian component is

$$\mathbf{A}^\alpha = \mathbf{K}\mathbf{\Lambda}^\alpha\mathbf{K}^{-1} .$$

The associated split flux component $\mathbf{F}^\alpha = \mathbf{A}^\alpha\mathbf{U}$ is

$$\mathbf{F}^\alpha = \frac{\rho}{2\gamma}\begin{bmatrix} \lambda_1^\alpha + 2(\gamma-1)\lambda_2^\alpha + \lambda_3^\alpha \\ (u-a)\lambda_1^\alpha + 2(\gamma-1)u\lambda_2^\alpha + (u+a)\lambda_3^\alpha \\ (H-ua)\lambda_1^\alpha + (\gamma-1)u^2\lambda_2^\alpha + (H+ua)\lambda_3^\alpha \end{bmatrix} , \tag{8.67}$$

where the eigenvalues λ_k^α are given by (8.32), for $\alpha = +, -$.

The Three–Dimensional Case

For the three–dimensional case we have

$$\mathbf{K}^{-1} = \frac{(\gamma-1)}{2a^2}\begin{bmatrix} H + \frac{a}{\hat{\gamma}}(u-a) & -(u + \frac{a}{\hat{\gamma}}) & -v & -w & 1 \\ -2H + \frac{4}{\hat{\gamma}}a^2 & 2u & 2v & 2w & -2 \\ -\frac{2va^2}{\hat{\gamma}} & 0 & \frac{2a^2}{\hat{\gamma}} & 0 & 0 \\ -\frac{2wa^2}{\hat{\gamma}} & 0 & 0 & \frac{2a^2}{\hat{\gamma}} & 0 \\ H - \frac{a}{\hat{\gamma}}(u+a) & -u + \frac{a}{\hat{\gamma}} & -v & -w & 1 \end{bmatrix} \tag{8.68}$$

and the resulting split flux component $\mathbf{F}^\alpha = \mathbf{A}^\alpha\mathbf{U}$ is found to be

$$\mathbf{F}^\alpha = \frac{\rho}{2\gamma}\begin{bmatrix} \lambda_1^\alpha + 2(\gamma-1)\lambda_2^\alpha + \lambda_5^\alpha \\ (u-a)\lambda_1^\alpha + 2(\gamma-1)u\lambda_2^\alpha + (u+a)\lambda_5^\alpha \\ v\lambda_1^\alpha + 2(\gamma-1)v\lambda_2^\alpha + v\lambda_5^\alpha \\ w\lambda_1^\alpha + 2(\gamma-1)w\lambda_2^\alpha + w\lambda_5^\alpha \\ (H-ua)\lambda_1^\alpha + (\gamma-1)\mathbf{V}^2\lambda_2^\alpha + (H+ua)\lambda_5^\alpha \end{bmatrix} . \tag{8.69}$$

Exercise 8.10. Verify expressions (8.68) and (8.69) above.

Solution 8.11. (Left to the reader).

8.4.3 The van Leer Splitting

Van Leer [560], [561] constructed a splitting for the Euler equations that has some extra desirable properties, namely

– (I) The split Jacobian matrices

$$\hat{\mathbf{A}}^{+} = \frac{\partial \mathbf{F}^{+}}{\partial \mathbf{U}} \ , \quad \hat{\mathbf{A}}^{-} = \frac{\partial \mathbf{F}^{-}}{\partial \mathbf{U}}$$

are required to be continuous.

– (II) The split fluxes are degenerate *for subsonic flow*, that is $\hat{\mathbf{A}}^{+}$, $\hat{\mathbf{A}}^{-}$ have a zero eigenvalue.

Van Leer expresses the flux vector $\mathbf{F}$ as a function of density, sound speed and Mach number $M = \frac{u}{a}$, that is

$$\mathbf{F} = \mathbf{F}(\rho, a, M) = \begin{bmatrix} \rho a M \\ \rho a^2 (M^2 + \frac{1}{\gamma}) \\ \rho a^3 M (\frac{1}{2} M^2 + \frac{1}{\gamma - 1}) \end{bmatrix} \equiv \begin{bmatrix} f_{\text{mas}} \\ f_{\text{mom}} \\ f_{\text{ene}} \end{bmatrix} \ . \tag{8.70}$$

For the mass flux

$$f_{\text{mas}} = \rho a M$$

one requires quadratics in M and the split mass fluxes are

$$f^{+}_{\text{mas}} = \frac{1}{4} \rho a (1 + M)^2 \ , \quad f^{-}_{\text{mas}} = -\frac{1}{4} \rho a (1 - M)^2 \ . \tag{8.71}$$

The momentum split fluxes are

$$f^{+}_{\text{mom}} = f^{+}_{\text{mas}} \frac{2a}{\gamma} [\frac{(\gamma - 1)}{2} M + 1] \ , \quad f^{-}_{\text{mom}} = f^{-}_{\text{mas}} \frac{2a}{\gamma} [\frac{(\gamma - 1)}{2} M - 1] \tag{8.72}$$

and the energy split fluxes are

$$f^{+}_{\text{ene}} = \frac{\gamma^2}{2(\gamma^2 - 1)} \frac{[f^{+}_{\text{mom}}]^2}{f^{+}_{\text{mas}}} \ , \quad f^{-}_{\text{ene}} = \frac{\gamma^2}{2(\gamma^2 - 1)} \frac{[f^{-}_{\text{mom}}]^2}{f^{-}_{\text{mas}}} \ . \tag{8.73}$$

In vector form we have

$$\mathbf{F}^{+} = \frac{1}{4} \rho a (1 + M)^2 \begin{bmatrix} 1 \\ \frac{2a}{\gamma} (\frac{\gamma - 1}{2} M + 1) \\ \frac{2a^2}{\gamma^2 - 1} (\frac{\gamma - 1}{2} M + 1)^2 \end{bmatrix} \ , \tag{8.74}$$

$$\mathbf{F}^{-} = -\frac{1}{4} \rho a (1 - M)^2 \begin{bmatrix} 1 \\ \frac{2a}{\gamma} (\frac{\gamma - 1}{2} M - 1) \\ \frac{2a^2}{\gamma^2 - 1} (\frac{\gamma - 1}{2} M - 1)^2 \end{bmatrix} \ . \tag{8.75}$$

For the x–split three dimensional Euler equations the split flux formulae are

$$\mathbf{F}^{+} = \frac{1}{4}\rho a(1+M)^2 \begin{bmatrix} 1 \\ \frac{2a}{\gamma}(\frac{\gamma-1}{2}M+1) \\ v \\ w \\ \frac{2a^2}{\gamma^2-1}(\frac{\gamma-1}{2}M+1)^2 + \frac{1}{2}(v^2+w^2) \end{bmatrix} , \tag{8.76}$$

and

$$\mathbf{F}^{-} = -\frac{1}{4}\rho a(1-M)^2 \begin{bmatrix} 1 \\ \frac{2a}{\gamma}(\frac{\gamma-1}{2}M-1) \\ v \\ w \\ \frac{2a^2}{\gamma^2-1}(\frac{\gamma-1}{2}M-1)^2 + \frac{1}{2}(v^2+w^2) \end{bmatrix} , \tag{8.77}$$

where the Mach number is still $M = \frac{u}{a}$.

Concerning stability, van Leer [560] gives the following practical stability condition

$$C_{\text{cfl}} \equiv \frac{\Delta t}{\Delta x}(\mid u \mid + a) \leq \frac{2\gamma + \mid M \mid (3-\gamma)}{\gamma+3} . \tag{8.78}$$

Note that $C_{\text{cfl}} = C_{\text{cfl}}(M)$ and that when $\gamma = 1.4$ we have

$$C_{\text{cfl}}^{\max} = 1 \text{ for } \mid M \mid = 1 , \quad C_{\text{cfl}}^{\min} = \frac{2\gamma}{\gamma+3} \approx 0.636\ldots , \text{ for } \mid M \mid = 0 . \tag{8.79}$$

Remark 8.12. The CFL condition for the explicit FVS scheme is more restrictive than that for the Godunov method, for which C_{cfl} is close to unity. See Sect. 6.3.2 of Chap. 6 for a discussion on the CFL condition.

8.4.4 The Liou–Steffen Scheme

A recent scheme that attempts to combine features from the Flux Vector Splitting and Godunov approaches is due to Liou and Steffen [328]. The scheme has been formulated in terms of the time–dependent Euler equations and relies on splitting the flux vector $\mathbf{F}$ into a *convective* component $\mathbf{F}^{(c)}$ and a *pressure* component $\mathbf{F}^{(p)}$. For the x–split three dimensional flux we have

$$\mathbf{F}(\mathbf{U}) = \begin{bmatrix} \rho u \\ \rho u^2 + p \\ \rho uv \\ \rho uw \\ u(E+p) \end{bmatrix} = \begin{bmatrix} \rho u \\ \rho u^2 \\ \rho uv \\ \rho uw \\ \rho uH \end{bmatrix} + \begin{bmatrix} 0 \\ p \\ 0 \\ 0 \\ 0 \end{bmatrix} \equiv \mathbf{F}^{(c)} + \mathbf{F}^{(p)} , \tag{8.80}$$

with the obvious definitions for the convective component $\mathbf{F}^{(c)}$ and the pressure component $\mathbf{F}^{(p)}$. By introducing the Mach number and enthalpy

$$M = \frac{u}{a}\,, \quad H = \frac{E+p}{\rho}$$

we write

$$\mathbf{F}^{(c)} = M \begin{bmatrix} \rho a \\ \rho a u \\ \rho a v \\ \rho a w \\ \rho a H \end{bmatrix} \equiv M \hat{\mathbf{F}}^{(c)}\,, \tag{8.81}$$

with the obvious notation for the vector $\hat{\mathbf{F}}^{(c)}$. In defining the intercell numerical flux $\mathbf{F}_{i+\frac{1}{2}}$, Liou and Steffen take

$$\mathbf{F}_{i+\frac{1}{2}} = \mathbf{F}^{(c)}_{i+\frac{1}{2}} + \mathbf{F}^{(p)}_{i+\frac{1}{2}}\,, \tag{8.82}$$

where the *convective flux component* is given by

$$\mathbf{F}^{(c)}_{i+\frac{1}{2}} = M_{i+\frac{1}{2}} \left[\hat{\mathbf{F}}^{(c)}\right]_{i+\frac{1}{2}} \tag{8.83}$$

with definition

$$[\bullet]_{i+\frac{1}{2}} = \begin{cases} [\bullet]_i & \text{if } M_{i+\frac{1}{2}} \geq 0\,, \\ [\bullet]_{i+1} & \text{if } M_{i+\frac{1}{2}} \leq 0\,. \end{cases} \tag{8.84}$$

Note that the flux vector in (8.83) is upwinded according to the sign of the convection, or advection, speed *implied* in the intercell Mach number $M_{i+\frac{1}{2}}$. For this reason Liou and Steffen call their scheme AUSM, which stands for Advection Upstream Splitting Method.

The cell–interface Mach number is given by the splitting

$$M_{i+\frac{1}{2}} = M_i^+ + M_{i+1}^- \tag{8.85}$$

with the positive and negative components yet to be defined. The splitting of the pressure flux component depends on the splitting of the pressure itself, namely

$$p_{i+\frac{1}{2}} = p_i^+ + p_{i+1}^-\,. \tag{8.86}$$

For the splitting of the Mach number Liou and Steffen follow van Leer and set

$$M^{\pm} = \begin{cases} \pm\frac{1}{4}(M \pm 1)^2 & \text{if } \mid M \mid \leq 1\,, \\ \frac{1}{2}(M \pm \mid M \mid) & \text{if } \mid M \mid > 1\,. \end{cases} \tag{8.87}$$

For splitting the pressure they suggest two choices, namely

$$p^{\pm} = \begin{cases} \frac{1}{2}p(1 \pm M) & \text{if } \mid M \mid \leq 1 \\ \frac{1}{2}p\frac{(M \pm \mid M \mid)}{M} & \text{if } \mid M \mid > 1 \end{cases} \tag{8.88}$$

and

$$p^{\pm} = \begin{cases} \frac{1}{4}p(M \pm 1)^2(2 \mp M) & \text{if } \mid M \mid \leq 1\,, \\ \frac{1}{2}p\frac{(M \pm \mid M \mid)}{M} & \text{if } \mid M \mid > 1\,. \end{cases} \tag{8.89}$$

For more details see the original paper by Liou and Steffen [328] and the more recent publication of Liou [327].

8.5 Numerical Results

Here we illustrate the performance of three FVS–type schemes on the one–dimensional, time dependent Euler equations for ideal gases with $\gamma = 1.4$, namely the Steger–Warming FVS scheme, the van Leer FVS scheme and the AUSM scheme of Liou and Steffen. Numerical results are compared with the exact solution. The respective results are obtained from running two codes of *NUMERICA* [519], namely HE–E1FVS (FVS schemes) and HE–E1RPEXACT (exact Riemann solver).

8.5.1 Tests

We use five test problems with exact solution. Data consists of two constant states $\mathbf{W}_{\mathrm{L}} = [\rho_{\mathrm{L}}, u_{\mathrm{L}}, p_{\mathrm{L}}]^T$ and $\mathbf{W}_{\mathrm{R}} = [\rho_{\mathrm{R}}, u_{\mathrm{R}}, p_{\mathrm{R}}]^T$, separated by a discontinuity at a position $x = x_0$, and are given in Table 8.1. The exact and numerical solutions are found in the spatial domain $0 \leq x \leq 1$. The numerical solution is computed with $M = 100$ cells. The Courant number coefficient is taken as $C_{\mathrm{cfl}} = 0.9$, except for the van Leer scheme, for which we took $C_{\mathrm{cfl}} = 0.6$. In implementing the CFL condition we use the simple formula given by equation 6.20 of Chap. 6 to estimate the maximum wave speed. Therefore, for all methods, we reduce the CFL number further to 0.2 of that given by the CFL condition, for the first 5 time steps. Boundary conditions are transmissive. For each test problem we select a convenient position x_0 of the initial discontinuity and the output time; these are stated in the legend of each figure displaying computational results. All numerical results should be compared with those from Godunov's method, Figs. 6.8 to 6.12 of Chap. 6. For more details on the exact solutions of the test problems see Sect. 4.3.3 of Chap. 4.

Test	ρ_{L}	u_{L}	p_{L}	ρ_{R}	u_{R}	p_{R}
1	1.0	0.75	1.0	0.125	0.0	0.1
2	1.0	-2.0	0.4	1.0	2.0	0.4
3	1.0	0.0	1000.0	1.0	0.0	0.01
4	5.99924	19.5975	460.894	5.99242	-6.19633	46.0950
5	1.0	-19.59745	1000.0	1.0	-19.59745	0.01

Table 8.1. Data for five test problems with exact solution. Test 5 is like Test 3 with negative uniform background speed

8.5.2 Results for Test 1

Test 1 is a *modified* version of the popular Sod's test [453]; the solution consists of a right shock wave, a right travelling contact wave and a left *sonic* rarefaction wave; this test is very useful in assessing the *entropy satisfaction*

property of numerical methods. Figs. 8.3 to 8.5 show the results for the three FVS schemes.

In the results from the Steger–Warming scheme, shown in Fig. 8.3, the resolution of the shock and the right travelling contact is comparable with that of Godunov's method, Fig. 6.8 of Chap. 6. The resolution of the left rarefaction is less satisfactory; the head and tail are visibly smeared and the sonic point, as expected, is not handled correctly. The results from the van Leer scheme, shown in Fig. 8.4, are virtually identical to those of Godunov's method of Fig. 6.8 for the rarefaction and contact, but the shock is broader. The performance at the sonic point is comparable with that of Godunov's method and better than that of the Steger–Warming scheme. The results from the Liou and Steffen scheme are shown in Fig. 8.5. In comparison with Godunov's method, the shock wave is more sharply resolved and the contact wave is similar but the resolution of the rarefaction is not as good, particularly near the sonic point.

8.5.3 Results for Test 2

The exact solution of Test 2 consists of two symmetric rarefaction waves and a trivial contact wave of zero speed; the *Star Region* between the non–linear waves is close to vacuum, which makes this problem a suitable test for assessing the performance of numerical methods for low–density flows [182]; this is the so called *123 problem* introduced in Sect. 4.3.3 of Chap. 4. Figs. 8.6 to 8.8 show the results for the three FVS schemes.

The results from the Steger–Warming scheme, shown in Fig. 8.6, are virtually identical to those of the Godunov method, Fig. 6.9 of Chap. 6. The results from the van Leer scheme, shown in Fig. 8.7, are also comparable with those from the Godunov method. The heads of the rarefactions are slightly more diffused. The Liou and Steffen scheme, Fig. 8.8, gives results that are comparable with those of Godunov's method and slightly more accurate than those from van Leer's scheme; in the vicinity of the trivial contact, where both density and pressure are close to zero, the results are somewhat erratic, see velocity and internal energy plots.

In view of the fact that Godunov–type methods with linearised Riemann solvers will fail for this test problem [182], it is quite remarkable to note that all three FVS–type schemes described in this chapter actually run and give, overall, good results.

8.5.4 Results for Test 3

Test 3 is designed to assess the robustness and accuracy of numerical methods; its solution consists of a strong right travelling shock wave of shock Mach number 198, a contact surface and a left rarefaction wave. Figs. 8.9 and 8.10 show the results for two FVS schemes.

The Steger–Warming result, shown in Fig. 8.9, is seen to be overall less accurate than the corresponding result from the Godunov method, shown in Fig. 6.10 of Chap. 6; the numerical solution has an unphysical dip behind the shock wave, which is more clearly seen in the velocity and pressure plots. The results from the van Leer scheme, shown in Fig. 8.10, are also less accurate than those from the Godunov method, but they are more accurate than the results from the Steger–Warming scheme. The Liou and Steffen scheme, as coded by the author, failed to give a solution at all for this very severe test problem, even when reducing the CFL number to a value as low as 0.1.

8.5.5 Results for Test 4

Test 4, as Test 3, is also designed to assess the robustness of numerical methods; data originates from two very strong shock waves travelling towards each other and the solution consists of three strong discontinuities travelling to the right; the left shock wave moves to the right very slowly, which adds another difficulty [406] to numerical methods. Figs. 8.11 to 8.13 show the results for the three FVS schemes.

The results from the Steger and Warming scheme, shown in Fig. 8.11, are overall comparable with those of Godunov's method shown in Fig. 6.11 of Chapter 6. The only visible difference is seen near the left slowly moving shock, and as expected, this is more diffused in the Steger–Warming result; however, it appears as if the low frequency oscillations seen in the Godunov results are significantly reduced in the Steger–Warming scheme. The results from the van Leer scheme, shown in Fig. 8.12, are comparable with those of Godunov's method and are more accurate than those from the Steger–Warming scheme. The slowly–moving shock is resolved with two interior cells, instead of one in the Godunov's method, but low–frequency spurious oscillations are just about visible. The results from the Liou and Steffen scheme, shown in Fig. 8.13, are comparable with the Godunov and van Leer results for this test; the fast right shock is more sharply resolved than with the other methods, but at the cost of an overshoot; the slowly moving left shock is slightly more smeared than in the van Leer result.

8.5.6 Results for Test 5

Test 5 is effectively Test 3, with a negative uniform background speed so as to obtain a stationary contact discontinuity. Test 5 is also designed to test the robustness of numerical methods but the main reason for devising this test is for assessing the ability of numerical methods to resolve *slowly–moving contact discontinuities*. The exact solution of Test 5 consists of a left rarefaction wave, a right–travelling shock wave (slow) and a *stationary* contact discontinuity. Figs. 8.14 to 8.16 show the results for the three FVS schemes and Fig. 8.17 shows the respective results obtained from the Godunov method used in conjunction with the exact Riemann solver, code HE–E1GODSTATE

of *NUMERICA* [519]. We note that at the chosen output time, the right travelling shock wave has propagated only 5 cells, in 81 time steps. For this test problem the results from the Steger/Warming and van Leer FVS schemes are similar, in that the contact discontinuity is heavily smeared, even for a relatively short evolution time. The Liou and Steffen FVS scheme, Fig. 8.16, differs from the other two FVS schemes in that it resolves the contact discontinuity more sharply; note however the unphysical oscillations in the vicinity of the shock wave, the contact discontinuity and even near the tail of the rarefaction. For comparison, the results from the Godunov method used in conjuction with the exact Riemann solver are displayed in Fig. 8.17. These are obviously superior to any of the FVS schemes, for this test problem.

The numerical experiments presented suggest that Flux Vector Splitting Schemes give, generally, results of similar quality to those obtained by the Godunov method. The difference between these two upwind approaches is evident when *slowly or stationary* contact waves are present. For multidimensional problems this has important implications for the accurate resolution of shear layers, material interfaces and vortical flows. The Liou and Steffen FVS–type scheme is an exception, as it does resolve contacts more accurately than the Warming–Beam and van Leer schemes, although there are questions marks about its robustness. For Test 3 the Liou and Steffen scheme *crashed* and for Test 5 produced large unphysical oscillations. It is worth remarking that the Godunov method was used in conjunction with the exact Riemann solver, to obtain the numerical results of Fig. 8.17. If the Godunov scheme is used with linearised Riemann solvers, then it would fail for low–density flows, such as Test 2 for example, whereas the FVS–type schemes appear to be much less sensitive; they all produced acceptable results for Test 2. In addition, if the Godunov method is used in conjunction with *incomplete* Riemann solvers, such as those that ignore the presence of linear waves in the structure of the solution of the Riemann problem, then the resolution of contacts will be as poor as that of FVS–type schemes, such as the Warming–Beam and van Leer schemes. The selection of the Riemann solver is crucial to the performance of the Godunov method. See Chaps. 9 to 12.

For details on how to extend FVS–type schemes to higher order of accuracy for one–dimensional homogeneous problems the reader is referred to Chapts. 13 and 14. Methods for treating source terms are given in Chapt. 15 and techniques to extend the methods to solve multidimensional problems are given in Chapt. 16. For multidimensional, steady state, applications of Flux Vector Splitting methods, readers are encouraged to consult, amongst many others, the following references: [12], [13], [600], [166], [578].

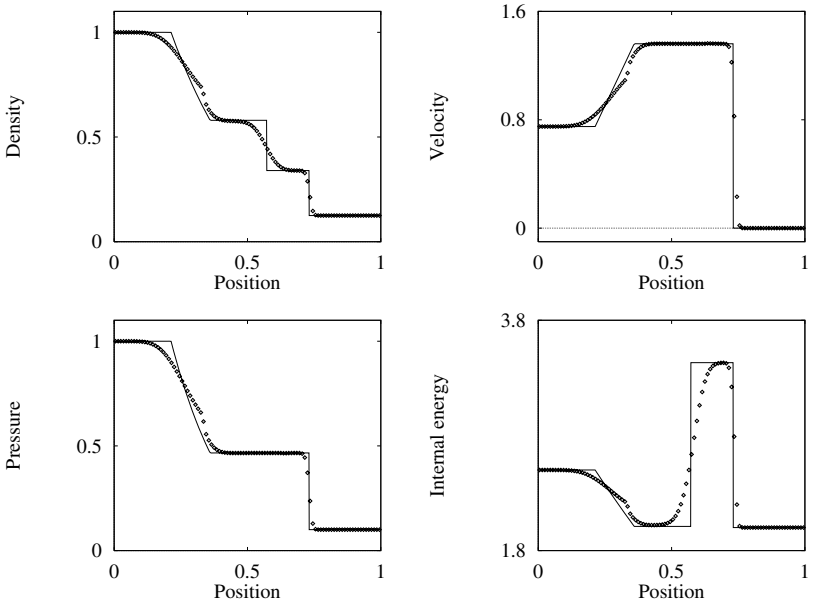

Fig. 8.3. Steger and Warming FVS scheme applied to Test 1, with $x_0 = 0.3$. Numerical (symbol) and exact (line) solutions are compared at time 0.2 units

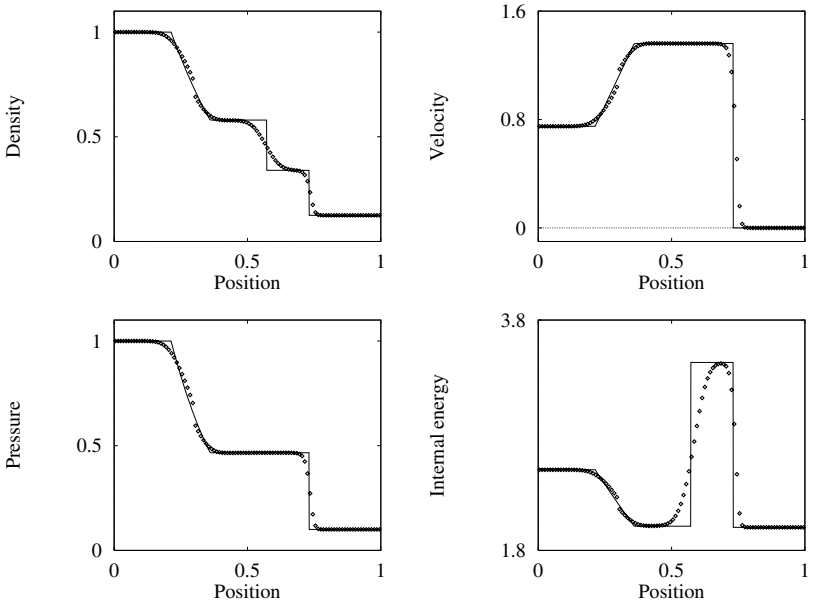

Fig. 8.4. Van Leer FVS scheme applied to Test 1, with $x_0 = 0.3$. Numerical (symbol) and exact (line) solutions are compared at time 0.2 units

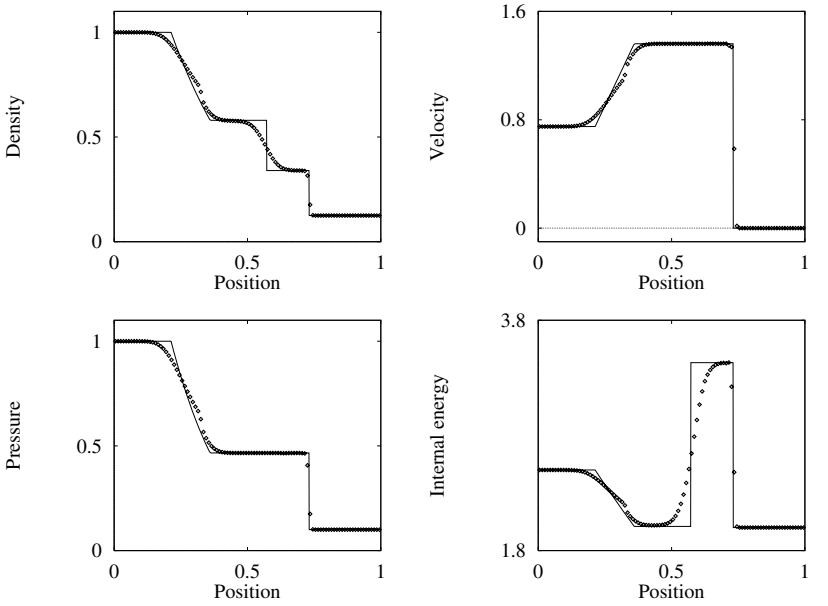

Fig. 8.5. Liou and Steffen scheme applied to Test 1, with $x_0 = 0.3$. Numerical (symbol) and exact (line) solutions are compared at time 0.2 units

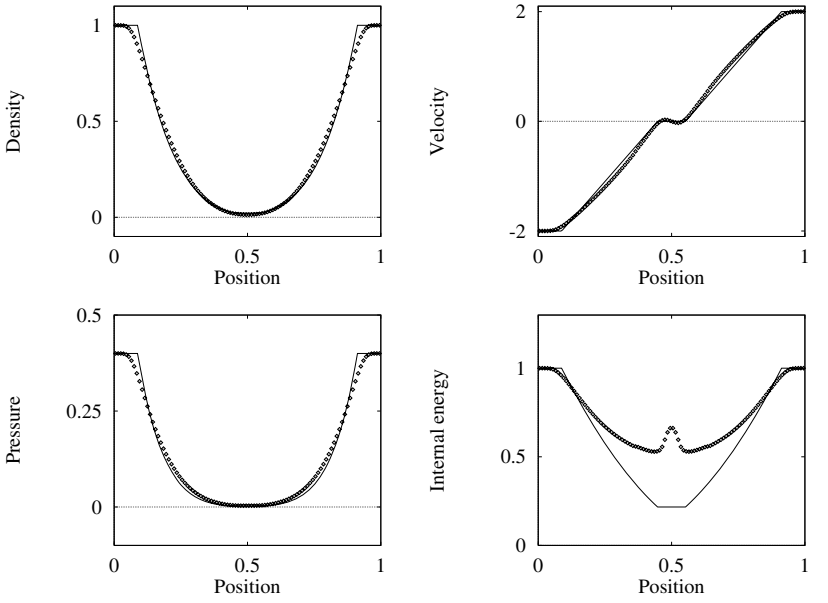

Fig. 8.6. Steger and Warming FVS scheme applied to Test 2, with $x_0 = 0.5$. Numerical (symbol) and exact (line) solutions are compared at time 0.15 units

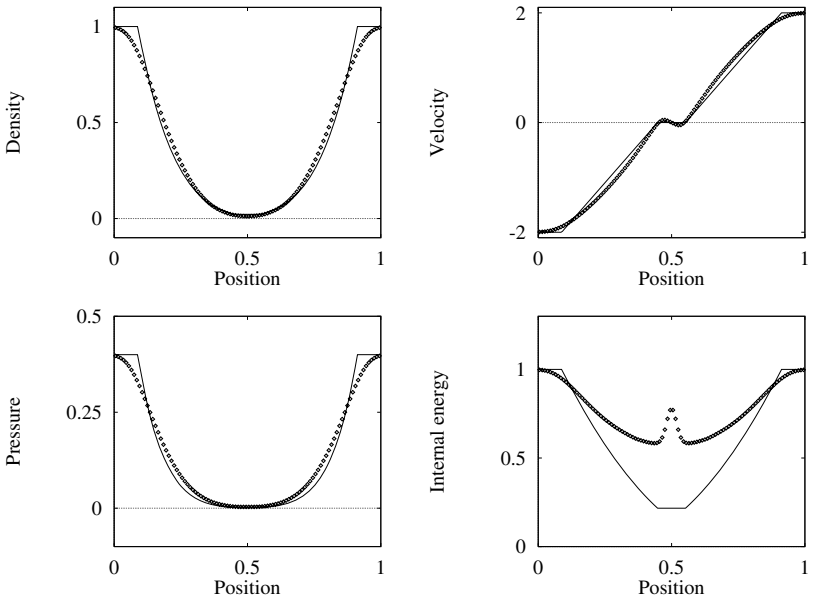

Fig. 8.7. Van Leer FVS scheme applied to Test 2, with $x_0 = 0.5$. Numerical (symbol) and exact (line) solutions are compared at time 0.15 units

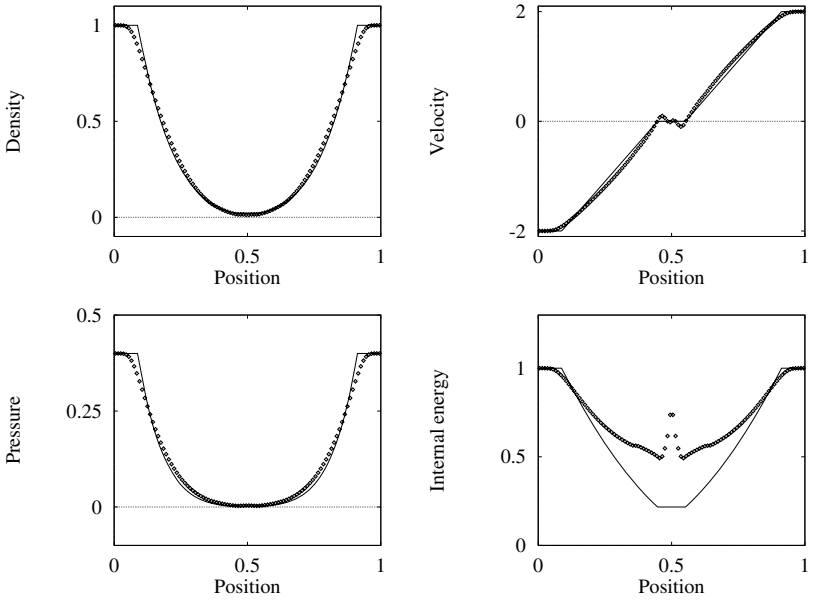

Fig. 8.8. Liou and Steffen scheme applied to Test 2, with $x_0 = 0.5$. Numerical (symbol) and exact (line) solutions are compared at time 0.15 units

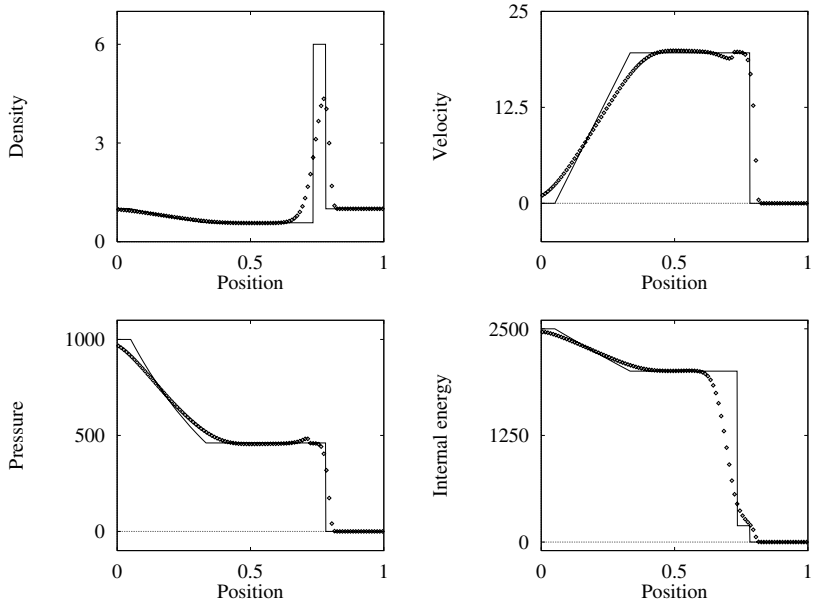

Fig. 8.9. Steger and Warming FVS scheme applied applied to Test 3, with $x_0 = 0.5$. Numerical (symbol) and exact (line) solutions are compared at time 0.012 units

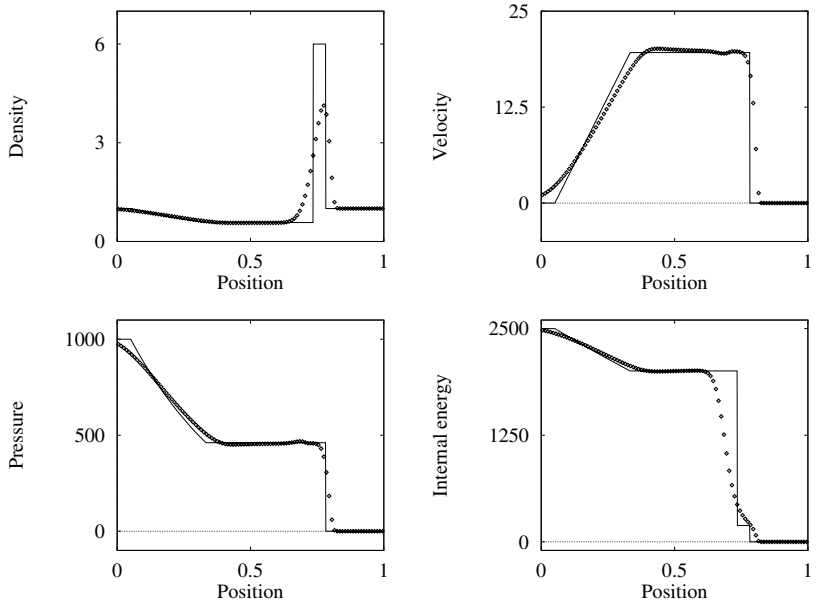

Fig. 8.10. Van Leer FVS scheme applied applied to Test 3, with $x_0 = 0.5$. Numerical (symbol) and exact (line) solutions are compared at time 0.012 units

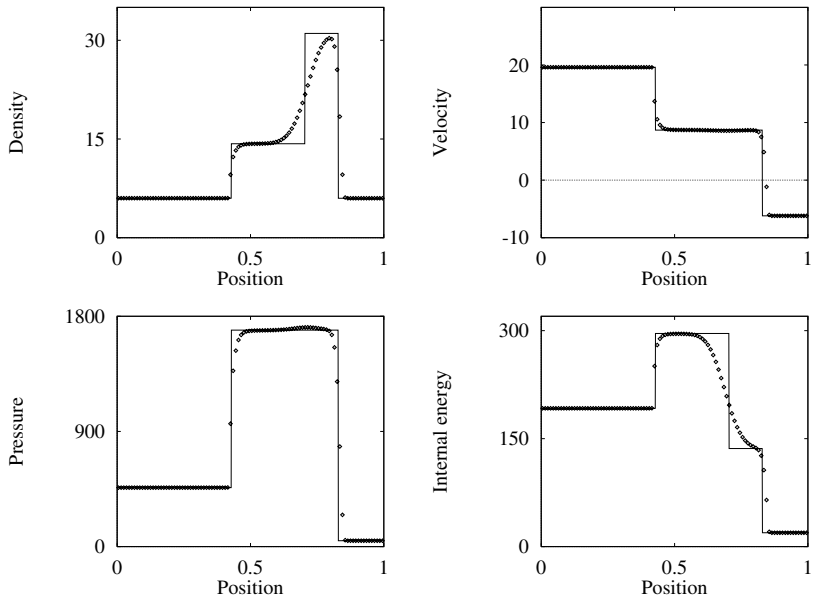

Fig. 8.11. Steger and Warming FVS scheme applied to Test 4, with $x_0 = 0.4$. Numerical (symbol) and exact (line) solutions are compared at time 0.035 units

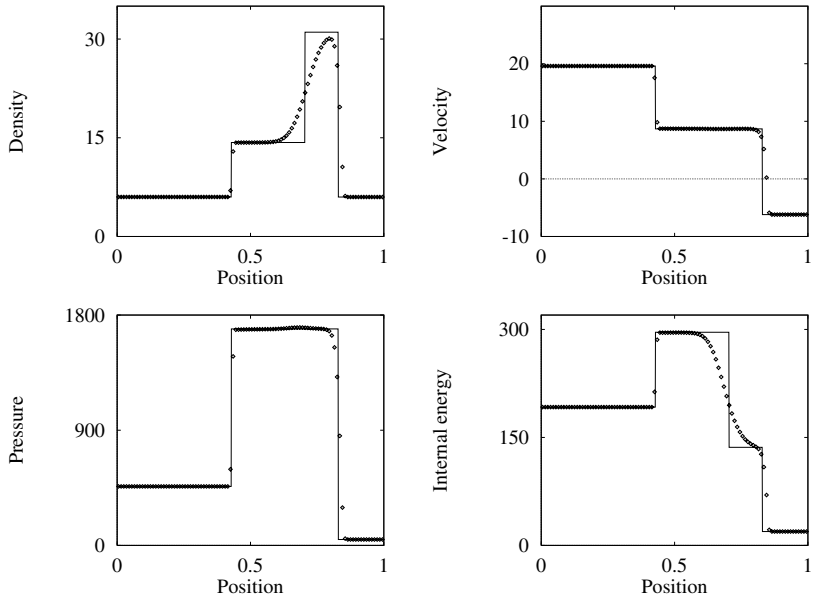

Fig. 8.12. Van Leer FVS scheme applied to Test 4, with $x_0 = 0.4$. Numerical (symbol) and exact (line) solutions are compared at time 0.035 units

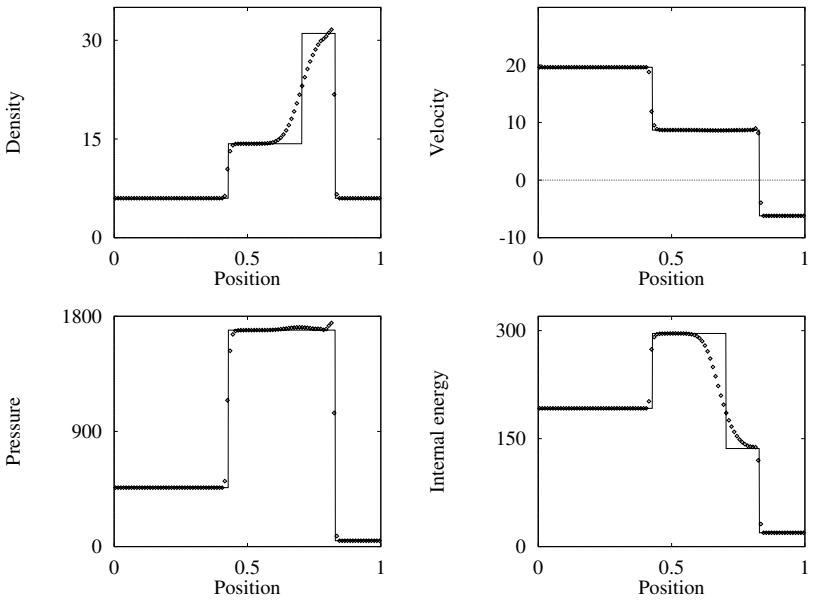

Fig. 8.13. Liou and Steffen scheme applied to Test 4, with $x_0 = 0.4$. Numerical (symbol) and exact (line) solutions are compared at time 0.035 units

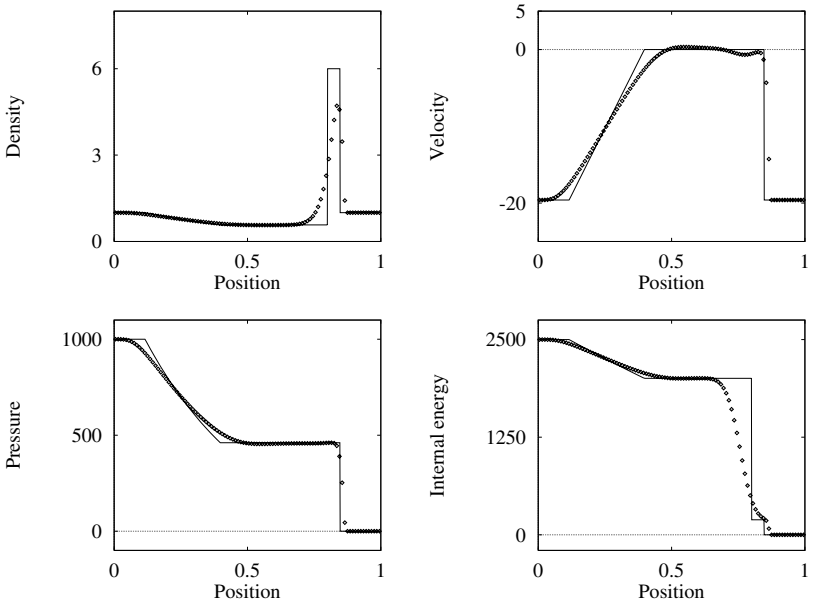

Fig. 8.14. Steger and Warming FVS scheme applied to Test 5, with $x_0 = 0.8$. Numerical (symbol) and exact (line) solutions are compared at time 0.012 units

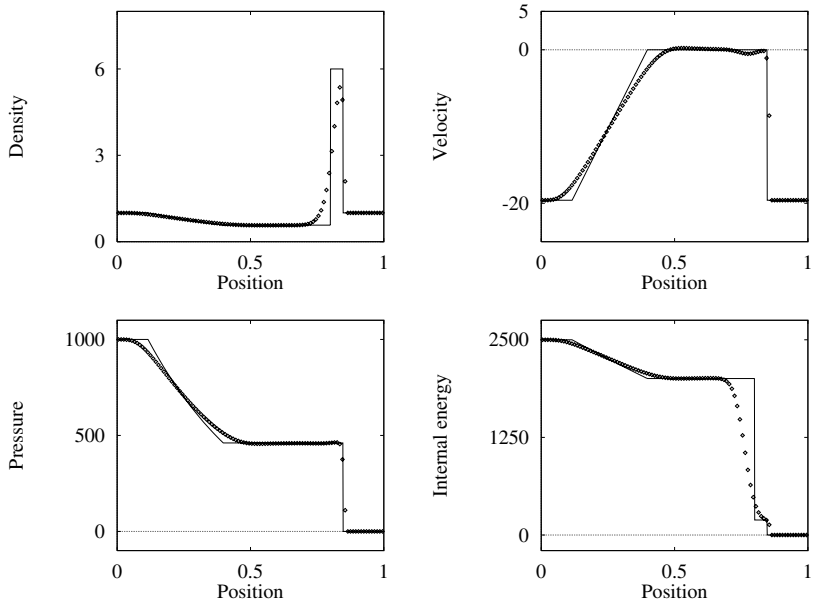

Fig. 8.15. Van Leer FVS scheme applied to Test 5, with $x_0 = 0.8$. Numerical (symbol) and exact (line) solutions are compared at time 0.012 units

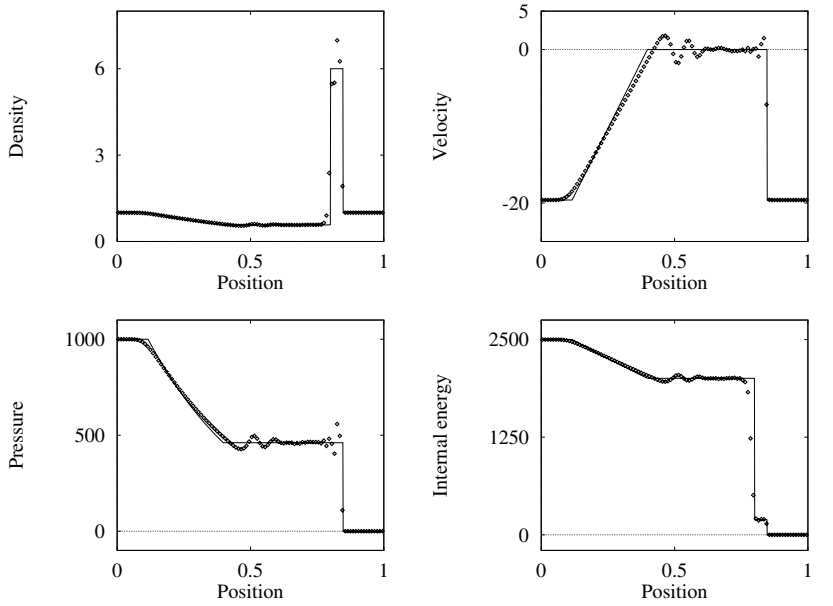

Fig. 8.16. Liou and Steffen scheme applied to Test 5, with $x_0 = 0.8$. Numerical (symbol) and exact (line) solutions are compared at time 0.012 units

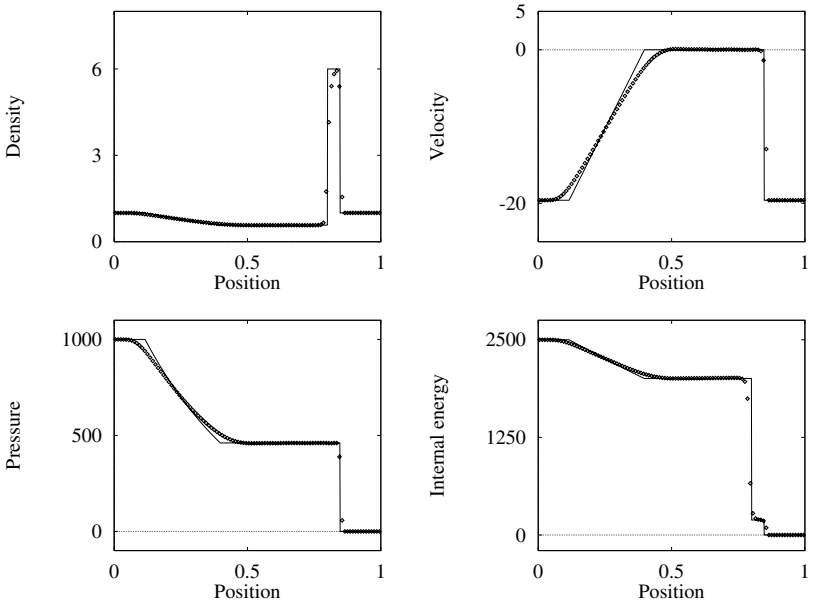

Fig. 8.17. Godunov scheme applied to Test 5, with $x_0 = 0.8$. Numerical (symbol) and exact (line) solutions are compared at time 0.012 units